JEM Journal of Experimental Medicine

BRIEF DEFINITIVE REPORT

# Targeting PLD2 in adipocytes augments adaptive thermogenesis by improving mitochondrial quality and quantity in mice

Hyung Sik Kim[1*], Min Young Park[1*], Nam Joo Yun[1], Hye Sun Go[2,3], Mi Young Kim[2,3], Je Kyung Seong[2,3], Minyoung Lee[4], Eun Seok Kang[4], Jaewang Ghim[5], Sung Ho Ryu[5], Brian A. Zabel[6], Ara Koh[5], and Yoe-Sik Bae[1]

**Phospholipase D (PLD)2 via its enzymatic activity regulates cell proliferation and migration and thus is implicated in cancer. However, the role of PLD2 in obesity and type 2 diabetes has not previously been investigated. Here, we show that during diet-induced thermogenesis and obesity, levels of PLD2 but not PLD1 in adipose tissue are inversely related with uncoupling protein 1, a key thermogenic protein. We demonstrate that the thermogenic program in adipose tissue is significantly augmented in mice with adipocyte-specific *Pld2* deletion or treated with a PLD2-specific inhibitor and that these mice are resistant to high fat diet–induced obesity, glucose intolerance, and insulin resistance. Mechanistically, we show that *Pld2* deletion in adipose tissue or PLD2 pharmacoinhibition acts via p62 to improve mitochondrial quality and quantity in adipocytes. Thus, PLD2 inhibition is an attractive therapeutic approach for obesity and type 2 diabetes by resolving defects in diet-induced thermogenesis.**

## Introduction

The global obesity epidemic is associated with a high risk of developing metabolic diseases including type 2 diabetes (Al-Goblan et al., 2014), insulin resistance (Makki et al., 2013; Ye, 2013), heart disease (Ebong et al., 2014; Poirier et al., 2006), stroke (Bazzano et al., 2010; Strazzullo et al., 2010), and hypertension (Hall et al., 2015; Jiang et al., 2016). When energy intake consistently exceeds total energy expenditure (EE), excess energy is stored in white adipocytes (Cohen and Spiegelman, 2016), whose expansion results in obesity (Vázquez-Vela et al., 2008). Thus, increasing EE under energy excess conditions is an attractive approach to combat obesity and obesity-associated diseases.

Adipose tissue has a major role in EE (Blaszkiewicz and Townsend, 2016; Saito, 2013). Classical brown adipose tissue (BAT) and beige adipose tissue can increase EE through non-shivering thermogenesis (van der Lans et al., 2013). This process relies mostly on uncoupling protein 1 (UCP1), a mitochondrial inner membrane protein that uncouples respiration from ATP synthesis and thus dissipates energy as heat (Cannon and Nedergaard, 2004; Sidossis and Kajimura, 2015). Conversely, reduced metabolic activity in BAT is associated with obesity (Orava et al., 2013), insulin resistance (Chondronikola et al., 2014), and cardiometabolic health (Becher et al., 2021) in humans. Thus, improving the metabolic activity or thermogenic potential of these adipose tissues is of important therapeutic interest.

Exposure to cold or excess caloric intake can induce adaptive thermogenesis, the latter also termed as diet-induced thermogenesis, both of which are known to be dependent on the sympathetic nervous system (SNS; Morrison et al., 2014) and stimulation of β-adrenergic receptors (βARs; Goto et al., 2016; Lowell and Bachman, 2003; Paulo et al., 2018; von Essen et al., 2017). Activation of diet-induced thermogenesis has been shown to preserve leanness in humans (Levine et al., 1999; Quatela et al., 2016; Saito et al., 2020). Thus, identification of causal molecular targets for defective diet-induced thermogenesis is actively ongoing and of important clinical relevance (Feldmann et al., 2009; Zhang et al., 2018).

Phospholipase D (PLD), which hydrolyzes phosphatidylcholine into phosphatidic acid (PA) and choline, plays an essential

[1]Department of Biological Sciences, Sungkyunkwan University, Suwon, Republic of Korea; [2]Laboratory of Developmental Biology and Genomics, College of Veterinary Medicine, Seoul National University, Seoul, Republic of Korea; [3]Korea Mouse Phenotyping Center, Seoul National University, Seoul, Republic of Korea; [4]Department of Internal Medicine, Yonsei University College of Medicine, Seoul, Republic of Korea; [5]Department of Life Science, Pohang University of Science and Technology, Pohang, Republic of Korea; [6]Palo Alto Veterans Institute for Research, Veterans Affairs Hospital, Palo Alto, CA.

*H.S. Kim and M.Y. Park contributed equally to this paper; Correspondence to Yoe-Sik Bae: yoesik@skku.edu; M. Park's present address is Drug Discovery Center, JW Pharmaceutical, Seoul, Republic of Korea; M. Kim's present address is Department of Biochemistry and Molecular Biology, Yonsei University College of Medicine, Seoul, Republic of Korea.

role in the regulation of cellular responses caused by diverse extracellular stimuli (Wang, 1999), leading to cell proliferation (Foster and Xu, 2003; Henkels et al., 2013) and cell migration (Gomez-Cambronero, 2014). The regulation of cellular responses by PLD is believed to be mediated by PA, which can bind to a variety of intracellular signaling molecules such as different kinases, phosphatases, and nucleotide-binding proteins (Jang et al., 2012; Steed and Chow, 2001). Accumulating evidence suggests that PLD is involved in the regulation of the pathological mechanism of several diseases, including cancer (Brown et al., 2017; Cho and Han, 2017), infections (Lee et al., 2015), pathological angiogenesis (Ghim et al., 2014), and neurodegenerative disorders such as Alzheimer's disease (Lindsley and Brown, 2012; Mendez-Gomez et al., 2018; Oliveira et al., 2010). However, the role of PLD in diet-induced thermogenesis and obesity has not been investigated so far. In this study, we discovered that PLD2 is expressed in adipose tissues, the expression of which is regulated by an excess calorie, high-fat diet (HFD). We thus sought to determine the role of PLD2 in adipocytes during diet-induced thermogenesis and obesity.

## Results and discussion

### PLD2 has an inverse relationship with UCP1 in adipose tissue

To investigate whether PLD plays a role in adipose tissue and obesity, we first determined if PLD isoforms are expressed in different adipose tissues. *Pld1* and *Pld2* mRNA levels were higher in inguinal white adipose tissue (ingWAT) and BAT than in epididymal white adipose tissue (epiWAT; Fig. 1 A). We next determined if expression of PLD isoforms changes during acute diet-induced thermogenesis and obesity. Consistent with a previous study (Ohtomo et al., 2017), UCP1 levels in BAT were increased by 4 wk of HFD but decreased after 12 wk of HFD, suggesting that a defect in acute diet-induced thermogenesis occurs after long-term HFD feeding. Interestingly, there was an inverse relationship between UCP1 and PLD2 levels in BAT from HFD-fed mice (Fig. 1 B). However, PLD1 was not detectable at protein levels, excluding a direct role for PLD1 in adipose tissue (Fig. 1 B). Similarly, in mice relieved from thermal stress at thermoneutral conditions (30°C), UCP1 levels were increased but PLD2 levels were decreased in BAT following 4 wk of HFD feeding (Fig. 1 C).

Diet-induced thermogenesis has been suggested to be mediated by the activation of the SNS and subsequent stimulation of βARs (Goto et al., 2016; Lowell and Bachman, 2003; Paulo et al., 2018). We thus investigated if the activation of the SNS and βARs is sufficient to suppress PLD2 levels. Cold exposure (for SNS and βAR activation) or β3AR agonist CL316,243 (CL) treatment at both room temperature and thermoneutrality significantly reduced the expression of PLD2, again showing an inverse relationship with UCP1 levels in BAT and ingWAT (Fig. 1, D and E). As expected, PLD activity was also reduced by the activation of SNS and βARs (Fig. 1 F).

A previous report showed that proteasomal activities are critical for the thermogenic ability of brown fat (Bartelt et al., 2018). Indeed, we found that 4 wk of HFD at thermoneutrality increased proteasomal activities in BAT and ingWAT (Fig. 1 G). β3AR antagonist SR59230A or proteasome inhibitor bortezomib, but not a lysosome inhibitor, chloroquine, reversed the βAR agonist isoprenaline-induced PLD2 reduction in primary brown adipocytes (Fig. 1, H and I). This suggested that increased proteasomal activity during diet-induced thermogenesis might induce PLD2 degradation. However, 12 wk of HFD feeding reversed the increased proteasomal activity (Fig. 1 J), consistent with the reversed UCP1 levels in mice on 12 wk of HFD (Fig. 1 B) compared with 4 wk of HFD. In addition, *Pld2* mRNA levels were increased in BAT and ingWAT by 12 wk of HFD (Fig. S1 A). This seems to reflect a compensatory increase of *Pld2* mRNA levels as a result of PLD2 degradation, since inhibition of PLD2 protein degradation blocked the isoprenaline-induced increase in *Pld2* mRNA levels (Fig. S1 B). Taken together, PLD2 degradation was observed during adaptive thermogenesis; however, blunted proteasomal activities and a compensatory increase of *Pld2* after a long-term HFD feeding might contribute to increased PLD2 expression in adipose tissue.

Although diet-induced adaptive thermogenesis occurs in response to excessive caloric intake to limit weight gain, prolonged high-calorie intake eventually leads to diet-induced obesity (Fischer et al., 2019; Rothwell and Stock, 1979; Saito et al., 2020). This suggests that there are factors regulated during adaptive thermogenesis that can exacerbate diet-induced obesity. In this study, we found degradation of PLD2 on BAT during adaptive thermogenesis. An isoprenaline-induced PLD2 decrease was blocked by bortezomib but not by chloroquine (Fig. 1 I), which suggests that the βAR agonist–stimulated PLD2 decrease is mediated by the proteasomal pathway in brown adipocytes. Furthermore, isoprenaline-induced PLD2 degradation is blocked by SR59230A (Fig. 1 H), suggesting a crucial role of β3AR in the process. Taken together, the results suggest that β3AR activation during adaptive thermogenesis may cause PLD2 degradation via the proteasomal pathway. To our knowledge, no reports have yet demonstrated PLD2 degradation in response to physiological stress or HFD feeding; thus, this is the first determination that PLD2 can be degraded during adaptive thermogenesis. A detailed molecular mechanism regarding PLD2 degradation during adaptive thermogenesis should be investigated in future studies.

### PLD2 regulates the thermogenic program in adipose tissues

Based on the inverse relationship between PLD2 and UCP1 levels, we asked if PLD2 inhibits the thermogenic program in adipose tissue. Thus, we generated adipocyte-specific *Pld2* conditional KO (hereafter referred to as *Pld2* Ad-KO) mice (Fig. S1 C). 8-wk-old *Pld2* Ad-KO mice showed almost complete depletion of PLD2 in different adipose tissues (epiWAT, ingWAT, and BAT) but not in the liver without differences in body weight when on a chow diet (Fig. S1, D and E). In *Pld2* Ad-KO mice, ingWAT and BAT showed a darker red (brown) color and higher induction of mitochondrial and thermogenic program genes compared with control littermates (Fig. 2, A and B), which was also supported by H&E and UCP1 histological staining (Fig. 2 C). Supporting a role for PLD2 in the thermogenic program, *Pld2* Ad-KO mice displayed higher temperatures in BAT and maintained higher rectal temperatures during a 4-h cold exposure than their littermate controls (Fig. 2, D and E). In addition, mice injected

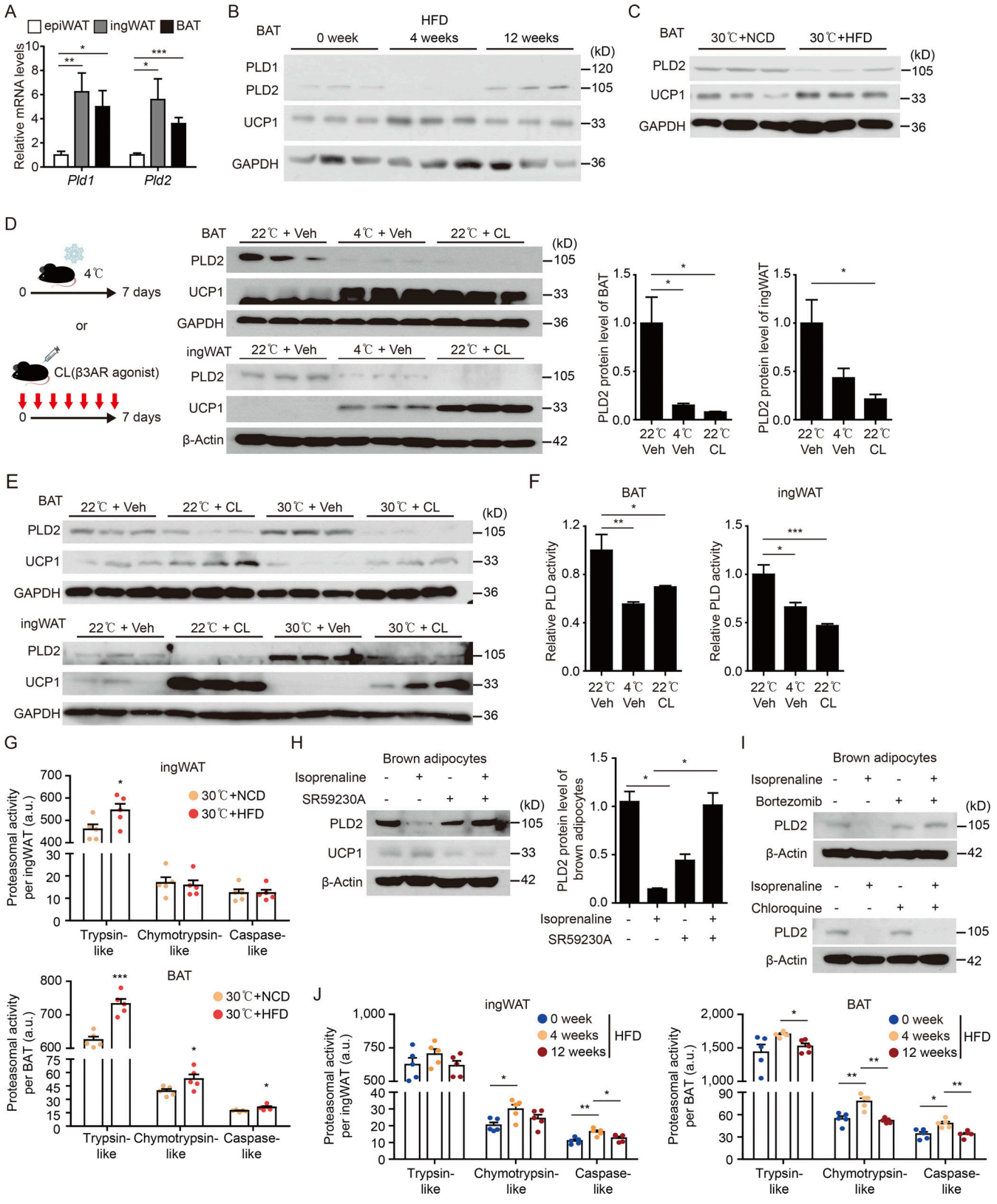


Figure 1. **An inverse relationship between PLD2 and UCP1 expression in adipose tissues upon HFD feeding. (A)** Quantitative RT-PCR of *Pld1* and *Pld2* mRNA expression in various adipose tissues from 8-wk-old WT mice ($n$ = 6/group). **(B)** Representative Western blot images of PLD1, PLD2, UCP1, and GAPDH in BAT from HFD (60% fat)-fed WT mice for 0, 4, and 12 wk at 22°C. **(C)** Representative Western blot images of PLD2, UCP1, and GAPDH in BAT from NCD or HFD (45% fat)-fed WT mice for 4 wk at 30°C. **(D)** Experiments to test the effects of sympathetic nerve system stimulation on the level of PLD2. Schematic illustration depicting WT mice incubated at 4°C for 1 wk or injected with the β3AR agonist, CL, at 1 mg/kg for 7 consecutive days (left). Representative Western blot images of PLD2, UCP1, GAPDH, and β-Actin (middle), and quantification of PLD2 protein level (right) in BAT and ingWAT ($n$ = 6/group). **(E)** Representative

Western blot images of PLD2, UCP1, and GAPDH in BAT and ingWAT from vehicle- or CL-stimulated mice at 22°C or 30°C for 1 wk. **(F)** PLD activity levels in lysates of BAT and ingWAT from 8-wk-old WT mice incubated at 4°C for 1 wk or injected with CL at 1 mg/kg for 7 consecutive days ($n$ = 6/group). **(G)** The proteasomal activity in the lysates of ingWAT and BAT from NCD or HFD (45% fat)-fed WT mice for 4 wk at 30°C ($n$ = 5/group). **(H)** Representative Western blot images of PLD2, UCP1, and β-Actin (left) and quantification of PLD2 (right) in isoprenaline (1 μM)- and SR59230A (1 μM)-treated primary brown adipocytes. **(I)** Representative Western blot images of PLD2 and β-Actin in isoprenaline (1 μM)-, bortezomib (20 nM)-, and chloroquine (10 μM)-treated primary brown adipocytes. **(J)** The proteasomal activity in the lysates of ingWAT and BAT from HFD (60% fat)–fed WT mice for 0, 4, and 12 wk at 22°C ($n$ = 5/group). The data are presented as mean ± SEM. *, P < 0.05; **, P < 0.01; ***, P < 0.001 by two-tailed Student's $t$ test (A, D [right], F, G, H [right], and J). Data are representative of at least two (C, E, H, and I) or three independent experiments (A, B, D, F, G, and J). a.u., arbitrary unit; Veh, vehicle.

with PLD2-specific inhibitor CAY10594 for 7 d also produced thermogenic brown and beige fats (Fig. 2, F–H; and Fig. S1 F), similar to those in *Pld2* Ad-KO mice, proposing that PLD2 enzymatic activity is involved in the thermogenic activation of adipose tissue.

Thermogenic activation of BAT is known to increase EE (Cannon and Nedergaard, 2011). As expected, depletion or inhibition of PLD2 in adipose tissue increased EE (normalized to lean body mass) during the dark phase without affecting respiratory exchange ratio (RER), locomotor activity, or food intake (Fig. 2, I–L; and Fig. S1, G–I). At thermoneutrality, inhibition of PLD2 also increased EE during both day and night compared with control mice, without affecting RER and locomotor activity (Fig. S1, J–L). In addition, the maximum thermogenic capacity was significantly higher in *Pld2* Ad-KO mice than control littermates at 22°C or at thermoneutral conditions when it was assessed after a single injection of βAR agonist CL (Fig. 2 M and Fig. S1 M). Similarly, PLD2 depletion increased EE in mice fed an HFD for 6 wk (Fig. S1 N). Taken together, these results suggest that PLD2 in adipose tissue inhibits EE by suppressing its thermogenic capacity.

### Adipocyte PLD2 ablation or pharmacoinhibition confers resistance to HFD-induced obesity and insulin resistance

Increased EE via thermogenic activation of adipose tissue has emerged as a promising therapeutic approach to combat obesity and insulin resistance (Kajimura et al., 2015). We thus investigated the therapeutic effects of CAY10594 in mice after inducing mild obesity (Fig. 3 A). 10 wk of CAY10594 administration in obese mice prevented weight gain without affecting food intake (Fig. 3, B–D). Inhibition of PLD2 activity in obese mice significantly reduced fat mass and the tissue weight of epiWAT, ingWAT, and liver (Fig. 3, E and F). Well-known phenotypes of HFD-induced obesity such as histological evidence of fatty liver and adipocyte hypertrophy (Muir et al., 2016; Sarwar et al., 2018) were prevented in CAY10594-injected mice on an HFD (Fig. 3 G). In addition, liver damage was also reduced by PLD2 inhibition in obese mice, as determined by plasma aspartate transaminase (AST) and alanine aminotransferase (ALT) levels (Fig. S2 A). Consistent with reduced adiposity, CAY10594 injection in obese mice enhanced EE during the dark phase (Fig. 3 H) without affecting RER and locomotor activity (Fig. S2, B and C). Importantly, PLD2 inhibition during diet-induced obesity significantly improved oral glucose tolerance and insulin sensitivity (Fig. 3, I and J); a similar improvement in glucose tolerance and insulin sensitivity was observed when the bolus of injected glucose or insulin was based on lean mass (Fig. S2, D and E). Low-grade inflammation in adipose tissue has been implicated in insulin resistance (Makki et al., 2013). PLD2 inhibition decreased the levels of proinflammatory genes (*Tnfa*, *Il6*, and *Il1b*) and increased anti-inflammatory gene (*Il10*) expression (Fig. S2 F).

We next investigated the effects of adipocyte-specific deletion of *Pld2* on HFD-induced obesity. *Pld2* Ad-KO mice were resistant to HFD-induced obesity compared with control mice (Fig. 3, K and L), although food intake was not different (Fig. 3 M). As expected, there was a reduction in fat mass, adipose tissue weight, and lipid accumulation in adipose tissue and the liver from *Pld2* Ad-KO mice compared with control littermates on an HFD for 12 wk (Fig. 3, N–R). PLD2 depletion in adipose tissue reduced glucose and insulin levels regardless of feeding or fasting (Fig. 3, S and T). Consistently, there was an improvement in glucose metabolism and insulin sensitivity (Fig. 3, U and V) in HFD-fed *Pld2* Ad-KO mice compared with control mice, although metabolic rates were not different between two groups after long-term HFD feeding (Fig. S2, G–I). Improved glucose tolerance and insulin sensitivity were maintained even when glucose or insulin was given to mice based on their lean mass (Fig. S2, J and K). Adipocyte-specific deletion of PLD2 also enhanced insulin-stimulated Akt and GSK3β phosphorylation, a key signaling axis that mediates the metabolic action of insulin (Fig. 3 W), and reduced the expression of proinflammatory genes in epiWAT (Fig. S2 L). These results indicate that targeting PLD2 activity prevents diet-induced obesity and glucose intolerance.

Since activated βAR was shown to up-regulate transcriptional activation of thermogenic genes including *Ucp1* (Chaudhry and Granneman, 1999; Goto et al., 2016; Inagaki et al., 2016), extensive efforts have been made to activate adipose tissue thermogenesis using selective β3AR agonists as an anti-obesity medication (Cypess et al., 2015; Lowell and Flier, 1997). However, these attempts have been unsuccessful, partly because of poor bioavailability and concern that pharmacological βAR activation leads to an increase in blood pressure (Michel et al., 2020; Michel et al., 1990), a major risk factor for cardiovascular disease (Ali et al., 2020; Madamanchi, 2007). Thus, identification of mechanisms that ensure readiness of mature BAT for immediate heat production and alternative routes for promoting beige fat bypassing the βAR signaling pathway could lead to therapeutic interventions with reduced cardiovascular risks. In this study, we found that depletion or inhibition of PLD2 during diet-induced obesity limited weight gain and improved glucose tolerance and insulin sensitivity. Taken together, derepression of PLD2 during adaptive thermogenesis seems to contribute to defective thermogenesis and obesity. Thus, it may be clinically relevant and important to determine whether PLD2 inhibitor

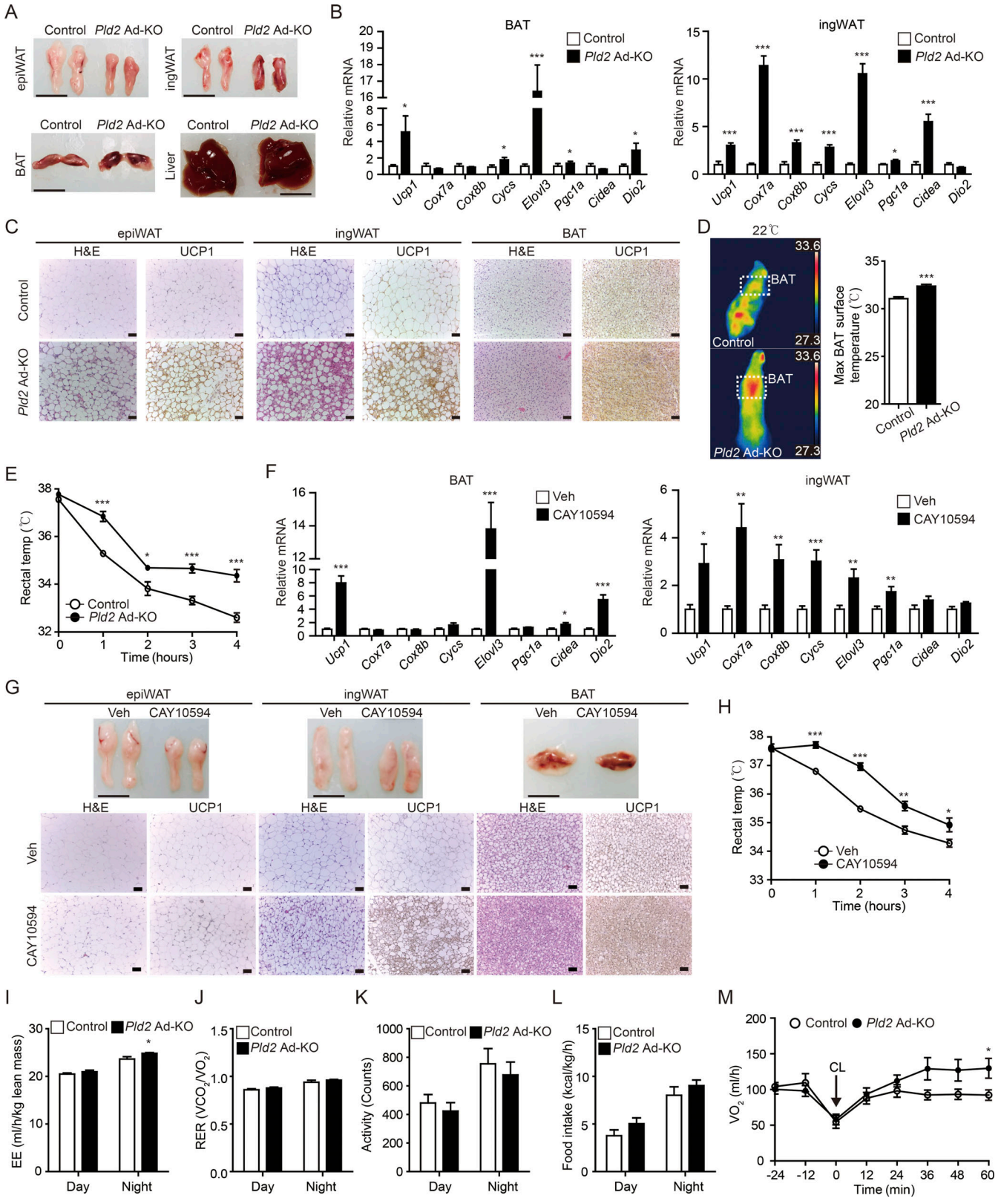


Figure 2. **Adipocyte-specific PLD2 deficiency or pharmacoinhibition activates the thermogenic program in adipose tissues. (A)** Representative images of fat depots and liver from 8-wk-old control and *Pld2* Ad-KO mice ($n$ = 6/group). Scale bars, 1 cm. **(B)** Relative mRNA expression of the thermogenic genes in BAT and ingWAT from 8-wk-old control and *Pld2* Ad-KO mice ($n$ = 6/group). **(C)** Representative images of H&E and UCP1 staining of epiWAT, ingWAT, and BAT from 8-wk-old control and *Pld2* Ad-KO mice ($n$ = 6/group). Scale bars, 25 µm. **(D)** Representative thermal imaging (left) and highest temperature of the BAT surface (right) of 8-wk-old control and *Pld2* Ad-KO mice at 22°C ($n$ = 6/group). **(E)** Measurement of rectal temperature of 8-wk-old control and *Pld2* Ad-KO mice every hour in cold exposure ($n$ = 6/group). **(F)** Relative mRNA expression of thermogenic genes in BAT and ingWAT from vehicle- or CAY10594-injected (7 d)

8-wk-old WT mice ($n$ = 6/group). **(G)** Representative images of fat depots and H&E and UCP1 staining of epiWAT, ingWAT, and BAT tissues from vehicle- or CAY10594-injected (7 d) 8-wk-old WT mice ($n$ = 6/group). Scale bars, 1 cm (top), 25 µm (middle and bottom). **(H)** Measurement of rectal temperature of vehicle- or CAY10594-injected (7 d) 8-wk-old WT mice every hour in cold exposure ($n$ = 6/group). **(I–L)** The level of EE (I), RER (J), locomotor activity (K), and daily food intake (L) of 8-wk-old control and *Pld2* Ad-KO mice ($n$ = 5/group). **(M)** The oxygen uptake ($VO_2$) levels of CL-injected 8-wk-old control or *Pld2* Ad-KO mice at room temperature condition ($n$ = 6/group). The data are presented as mean ± SEM. *, P < 0.05; **, P < 0.01; ***, P < 0.001 by Student's $t$ test (B, D [right], F, and I) and two-way ANOVA (E, H, and M). Data are representative of three independent experiments (A–H). Temp, temperature; Veh, vehicle; $VCO_2$, carbon dioxide production.

CAY10594 is effective in subjects with obesity and type 2 diabetes without severe side effects.

### PLD2 regulates mitochondrial quality and quantity through p62

An adipocyte-specific role for PLD2 led us to examine its impacts on p62, since others have published that adipocyte-specific p62-deficient mice are obese and show a decreased metabolic rate by impaired thermogenesis (Fischer et al., 2020; Huang et al., 2021). Moreover, previous reports demonstrated that BAT mitochondrial homeostasis requires mitophagy (Lu et al., 2018), and p62 is important for controlling mitochondrial quality by modulating mitophagy (Liu et al., 2017). We examined the effects of adipocyte-specific *Pld2* deletion or inhibition on p62 expression in ingWAT and BAT of HFD-fed mice. *Pld2* Ad-KO and CAY10594-injected mice showed significantly increased levels of p62 and UCP1 in ingWAT and BAT (Fig. 4, A and B; and Fig. S3, A and B). To assess the direct role of PLD2 on p62 expression, we incubated primary brown adipocytes with CAY10594 for 3 h and 24 h. PLD2 inhibition significantly induced p62 expression at both protein and mRNA levels, similar to the effects of β3AR agonist CL (Fig. 4 C), suggesting a cell-autonomous role of PLD2 activity on p62. In addition, we demonstrated that p62 mediates the effects of PLD2 inhibition on UCP1 levels and thermogenic gene expression via p62 knockdown in primary brown adipocytes treated with CAY10594 (Fig. 4, D and E).

Based on the role of p62 in improving mitochondrial function (Seibenhener et al., 2013), we next asked if PLD2 also regulates mitochondrial function. CAY10594 enhanced the localization of p62 in mitochondria 3 h after CAY10594 treatment (Fig. 4 F). Analyses of transmission electron microscopy and mitochondrial DNA–to–nuclear DNA ratios revealed that PLD2 depletion or inhibition markedly increased mitochondrial number and mass compared with controls (Fig. 4, G–J; and Fig. S3, C and D). We next asked if, in addition to increasing mitochondrial quantity, targeting PLD2 could also improve mitochondrial quality. Palmitate has been shown to induce mitochondrial dysfunction by dissipating mitochondrial membrane potential (Hammerschmidt et al., 2019), which can be assessed by the mitochondrial membrane potential sensitive dye tetramethylrhodamine methyl ester (TMRM). As expected, palmitate increased the $TMRM^{low}$ population but decreased the $TMRM^{high}$ mitochondrial population in primary brown adipocytes, which was effectively reversed by the treatment of PLD2 inhibitor CAY10594 (Fig. 4 K). $TMRM^{high}$ cells have been shown to be efficient in terms of oxygen consumption rate (OCR), basal and maximal respiration, and spare respiratory capacity compared with $TMRM^{low}$ cells (Choi et al., 2018; Franco-Iborra and Tanji, 2020; Gambini et al., 2020). In line with this, inhibition or depletion of PLD2 in brown adipocytes significantly enhanced the rate of oxygen consumption and the degree of oligomycin insensitive respiration (Fig. 4, L–O; and Fig. S3, E and F). Collectively, PLD2 negatively modulates p62, mitochondrial function, and energetics. In addition, CAY10594-induced PLD2 inhibition decreased Drp1 phosphorylation at S637, a marker for mitochondria fusion; increased Drp1 phosphorylation at S616, a marker for mitochondria fission; and increased mitophagy-associated LC3B (Fig. S3, G and H). The results suggest that PLD2 is involved in multiple aspects of mitochondrial biology.

Mitochondrial quality control and homeostasis are associated with adipose tissue remodeling and HFD-induced obesity (Bournat and Brown, 2010). Thus, mitochondrial quality control has been regarded as an important target for treating metabolic diseases (Held and Houtkooper, 2015). In this study, we observed that adipocyte-specific deletion of *Pld2* causes p62 up-regulation and localization into mitochondria (Fig. 4, A–C and F). Up-regulation of p62 is associated with improved mitochondrial quality control through mitophagy (Müller et al., 2013). Between our results and previous reports, PLD2 seems to play an essential role in mitochondrial quality control by negatively regulating p62 in adipocytes, which is required for browning and beige adipocytes to increase EE.

In this study, we demonstrated that there is an inverse relationship between PLD2 and UCP1 levels during diet-induced adaptive thermogenesis and obesity. Through genetic deletion in adipose tissue or pharmacological inhibition of PLD2, we propose that PLD2 is a negative regulator for adipocyte thermogenesis and EE and a promising target to prevent obesity, insulin resistance, and glucose intolerance.

## Materials and methods

### Animals

All experiments involving mice were performed with the approval of the Institutional Review Committee for Animal Care and Use at Sungkyunkwan University. All studies used male C57BL/6J background mice. C57BL/6J mice were purchased from DBL, and adiponectin-Cre mice (AdipoQ-cre) were kindly provided by Prof. Hail Kim (Korea Advanced Institute of Science and Technology, Daejeon, Republic of Korea). The *Pld2* flox/flox mice were generated as previously reported (Ghim et al., 2014). *Pld2* flox/flox mice were bred with AdipoQ-cre knock-in mice to generate *Pld2* flox/flox AdipoQ-cre (*Pld2* Ad-KO) mice. The mice were housed on a 12:12-h light-dark cycle with ad libitum access to food and water at 22°C. For the obese mouse model and control mouse, mice at 8 wk old were fed either a normal chow diet (NCD; 10% fat as kcal; Research Diets) or HFD (60% fat as

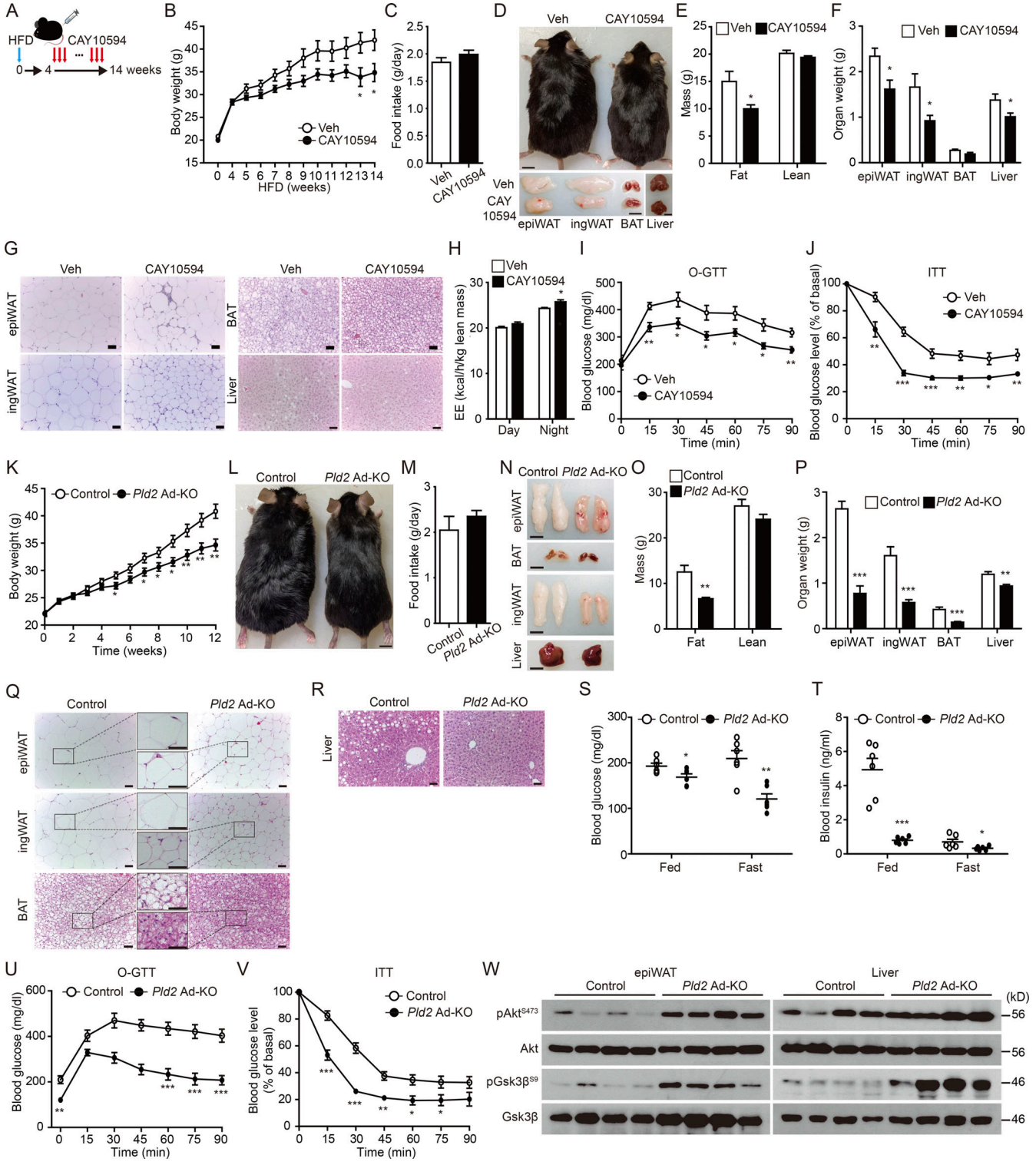


Figure 3. **Improvement of obesity and type 2 diabetes in PLD2-targeted mice. (A)** Schematic illustration of experiments to investigate the therapeutic effects of CAY10594 in obese mice. **(B and C)** Body weight curve (B) and daily food intake levels (C) of vehicle- or CAY10594-injected obese WT mice ($n$ = 6/group). **(D)** Representative images of mice (top), fat depots and liver (bottom) from vehicle- or CAY10594-injected obese mice ($n$ = 6/group). Scale bars, 1 cm. **(E)** Weights of fat and lean mass from vehicle- or CAY10594-injected obese mice ($n$ = 6/group). **(F)** Weights of fat depots and liver from vehicle- or CAY10594-injected obese mice ($n$ = 6/group). **(G)** Representative images of H&E staining of diverse fat depots and liver from vehicle- or CAY10594-injected obese mice. Scale bars, 25 µm. **(H)** Average EE at day and night from vehicle- or CAY10594-injected obese mice ($n$ = 6/group). **(I and J)** Blood glucose concentrations during O-GTT (I) and ITT (J) in fasted vehicle- or CAY10594-injected obese mice ($n$ = 6/group). **(K–M)** Body weight curve (K), representative images (L), and daily food intake levels (M) of HFD-induced control and *Pld2* Ad-KO mice for 12 wk ($n$ = 6/group). Scale bars, 1 cm. **(N)** Representative images of fat depots and liver of HFD-induced control and *Pld2* Ad-KO mice for 12 wk ($n$ = 6/group). Scale bars, 1 cm. **(O)** Weights of fat and lean mass of HFD-induced control and *Pld2* Ad-KO mice for 12 wk ($n$ = 6/group). **(P)** Weights of fat depots and liver from HFD-induced control and *Pld2* Ad-KO mice for 12 wk ($n$ = 6/group).

**(Q and R)** Representative images of H&E staining of diverse fat depots (Q) and liver (R) from HFD-induced control and *Pld2* Ad-KO mice for 12 wk ($n$ = 6/group). **(S and T)** Fed and fasted blood concentrations of glucose (S) and insulin (T) from HFD-induced control and *Pld2* Ad-KO mice for 12 wk ($n$ = 6/group). **(U and V)** Blood glucose concentrations during O-GTT (U) and ITT (V) in fasted HFD-induced control and *Pld2* Ad-KO mice for 12 wk ($n$ = 6/group). **(W)** Representative Western blot images of $pAkt^{S473}$, Akt, $pGsk3\beta^{S9}$, and Gsk3β in epiWAT and liver from HFD-induced control and *Pld2* Ad-KO mice for 12 wk. The data are presented as mean ± SEM. *, P < 0.05; **, P < 0.01; ***, P < 0.001 by two-way ANOVA (B, I–K, U, and V) or two-tailed Student's $t$ test (C, E, F, H, O, P, S, and T). Data are representative of three independent experiments (A–W). Veh, vehicle.

kcal; Research Diets) for 10 or 12 wk. For the diet-induced thermogenesis model that had down-regulated functional activity of BAT, mice at 8 wk old were fed an NCD for 4 wk in thermoneutrality condition (30°C). After inactivation of BAT, mice were fed an HFD (45% fat as kcal; Research Diets) for an additional 4 wk in thermoneutrality conditions.

### RNA isolation and quantitative RT-PCR

The total RNA was extracted from adipose tissues and primary adipocytes using the Trizol method (Invitrogen) following the manufacturer's instructions. Complementary DNA was prepared from 1 μg of RNA using the Reverse Transcription kit (iNtRON). PCR reactions were run in duplicate for each sample and analyzed using the Rotor-Gene SYBR Green PCR kit (Qiagen) and the Rotor-Gene Q 2plex real-time PCR instrument (Qiagen). mRNA expression levels were calculated using the ΔΔCT method and normalized to the housekeeping gene *Gapdh*. The primer sequences are provided in Table S1.

### Western blot analysis

Homogenized tissues and cells were lysed in RIPA buffer (iNtRON) containing protease and phosphatase inhibitors. Supernatants were prepared following a brief centrifugation, and protein concentrations in the supernatants were measured using the BCA Protein Assay Kit (Thermo Fisher Scientific). The cell lysates were then mixed with equal volumes of 2× SDS sample buffer and boiled at 95°C for 5 min. Next, the protein samples were separated by SDS-PAGE and transferred to a polyvinylidene difluoride membrane (Millipore). After blocking in a 5% skim milk solution or 4% BSA (Sigma-Aldrich), the membranes were incubated with the specific primary antibodies. Antibodies to UCP1, p62, DIO2, and PGC1-α were purchased from Abcam. Antibodies to pAkt (S473), Akt, pGsk3β (S9), Gsk3β, LC3B, pDRP1 (S616 or S637), Cytochrome C, β-Actin, and GAPDH were purchased from Cell Signaling Technology. Antibodies to DRP1 were from BD Bioscience, and anti-FIS1 antibodies were from Abnova. PLD antibody was kindly provided by Prof. Do Sik Min (Yonsei University, Incheon, Republic of Korea). After incubation, the membranes were washed with 1× Tris-buffered saline with 0.1% Tween 20 and incubated with anti-rabbit IgG HRP-linked antibody or anti-mouse IgG antibody, and the antigen–antibody complexes were visualized by enhanced chemiluminescence or Supersignal West Pico Chemiluminescent Substrate (Thermo Fisher Scientific). Densitometry was performed using Image J Software (National Institutes of Health).

### Proteasome activity assays

Proteolytic activities of proteasomes in lysates of ingWAT or BAT isolated from NCD- or HFD-fed mice bred in 22°C or 30°C environments were measured using the fluorogenic 7-amino-4-methylcoumarin (AMC)–conjugated peptide substrates. Each tissue was homogenized on ice using a IKA homogenizer in 300 μl lysis buffer containing 40 mM Tris-HCl (pH 7.6), 50 mM NaCl, 2 mM 2-mercaptoethanol, 2 mM ATP, 5 mM $MgCl_2$, and 10% glycerol, followed by sedimentation for 20 min at 17,000 *g*. The AMC fluorescence was monitored for 15 min at 37°C with the following peptides: 100 μM Suc-LLVY-AMC (substrate for the chymotrypsin-like proteasomal activity), 50 μM Boc-LRR-AMC (substrate for the trypsin-like activity), and 250 μM Z-LLE-AMC (substrate for the caspase-like activity), purchased from UBPBio.

### Measurement of PLD activity

PLD activity in adipose tissues was measured using the Amplex Red Phospholipase D Assay Kit (Invitrogen). In this assay, PLD cleaves phosphatidylcholine to yield choline and PA. The choline is then oxidized by choline oxidase to betaine and $H_2O_2$. Finally, in the presence of HRP, the $H_2O_2$ reacts with Amplex Red reagent to produce the fluorescent product resorufin, which is measured at 571 and 585 nm.

### Measurement of levels of plasma AST and ALT

The plasma levels of AST and ALT isolated from vehicle- or CAY10594-injected HFD-induced obese model mice were measured using commercially available kits from FUJIFILM according to the manufacturer's protocol.

### Histological and immunohistochemical analysis

Tissues were fixed in 4% paraformaldehyde (Sigma-Aldrich) for 60–72 h at room temperature and sectioned after being paraffin-embedded. Multiple sections were deparaffinized, rehydrated, and used for H&E staining and immunohistochemistry. For antigen retrieval, the slides were sunk in 10 mM sodium citrate (pH 6.0) and heated to 70°C for 30 min. Visualization of UCP1 was performed using a VECTASTAIN ABC Kit (Vector Laboratories) according to the manufacturer's instructions. Briefly, the slides were incubated with 5% normal goat serum for 30 min at room temperature to block nonspecific binding. The sections were incubated with primary antibody against UCP1 (Abcam) for 1 h at room temperature followed by 30 min incubation with a species-specific, biotinylated secondary antibody. The slides were incubated with alkaline phosphatase substrate (Vector Laboratories) for visualization.

### Metabolic cage analysis

Metabolic cage analysis was performed at Seoul University College of Veterinary Medicine, Korea Mouse Phenotyping Center. Metabolic rates including food consumption, oxygen

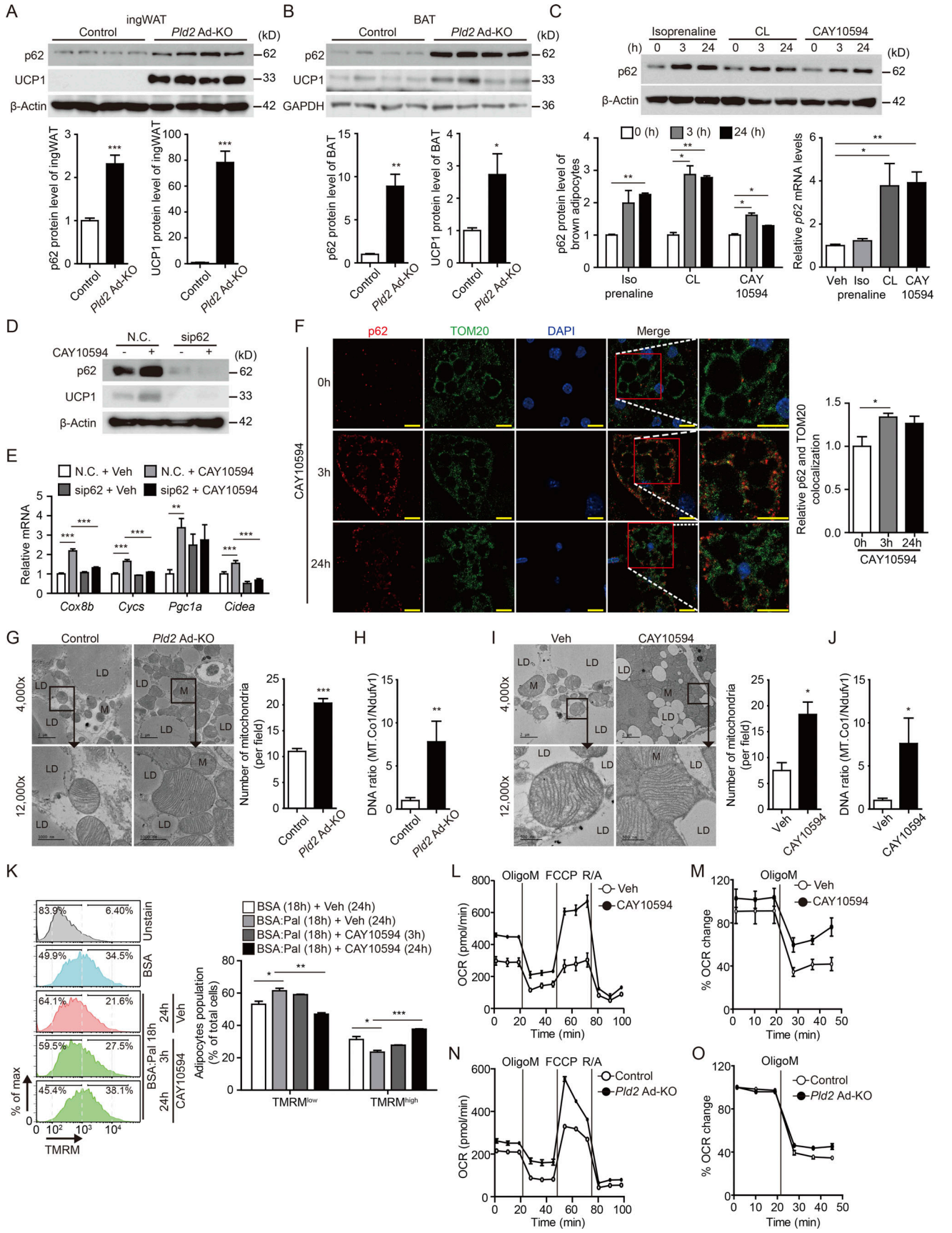


Figure 4. **Regulation of mitochondrial quality and quantity through p62 in adipocyte-specific *Pld2*-ablated or PLD2-pharmacoinhibited mice. (A and B)** Representative Western blot images (top) and quantification (bottom) of p62, UCP1, and β-Actin or GAPDH in ingWAT (A) and BAT (B) from HFD-induced

control and *Pld2* Ad-KO mice for 12 wk (*n* = 4/group). **(C)** Representative Western blot images (top) and quantification (bottom, left) of p62, β-Actin, and quantitative analysis (bottom, right) of *p62* mRNA expression in primary brown adipocytes treated with isoprenaline (1 μM), CL (10 μM), and CAY10594 (10 μM) at the indicated time points (*n* = 3/group). **(D and E)** Representative Western blot images of p62, UCP1, and β-Actin (D) or mRNA expression of thermogenic genes (E) in primary brown adipocytes transfected with a negative control siRNA (N.C.) or siRNA against p62 and treated with CAY10594 (10 μM) at 24 h. **(F)** Differentiated primary brown adipocytes were treated with CAY10594 (10 μM) for 0, 3, or 24 h. Immunostained (left) with anti-p62 (red), anti-TOM20 (green), and DAPI (blue) and quantitative analysis (right) of p62 and TOM20 colocalization (*n* = 3/group). Scale bars, 10 μm. **(G and H)** Representative images of transmission electron microscopy (G, left), mitochondria number (G, right), and relative ratio of mitochondrial DNA (*mt-Co1*) to nuclear DNA (*Ndufv1*; H) of BAT from HFD-induced control and *Pld2* Ad-KO mice for 12 wk (*n* = 6/group). LD, lipid droplet; M, mitochondria. Scale bars, 2 μm (top), 1 μm (bottom). **(I and J)** Representative images of transmission electron microscopy (I, left), mitochondria number (I, right), and relative ratio of mitochondrial DNA (*mt-Co1*) to nuclear DNA (*Ndufv1*; J) of BAT from vehicle- or CAY10594-injected obese mice (*n* = 6/group). Scale bars, 2 μm (top), 500 nm (bottom). **(K)** Representative TMRM analysis (left) and TMRM low or high population (right) of stimulated primary brown adipocytes with vehicle- or CAY10594 (10 μM) at the indicated times with palmitate (Pal, 500 μM) stimulation (*n* = 3/group). **(L)** Representative seahorse extracellular flux assays measuring OCR in primary brown adipocytes treated with vehicle or CAY10594 (10 μM) for 5 d (*n* = 3/group). **(M)** Representative measurements of the percentage change in OCRs in primary brown adipocytes treated with vehicle or CAY10594 (10 μM) for 5 d after injection of oligomycin, as an index of uncoupled respiration. The OCR before oligomycin injection was set as 100% (*n* = 3/group). **(N)** Representative seahorse extracellular flux assays measuring OCR in primary brown adipocytes from control and *Pld2* Ad-KO mice (*n* = 3/group). **(O)** Representative measurements of the percentage change in OCRs in primary brown adipocytes from control and *Pld2* Ad-KO mice after injection of oligomycin, as an index of uncoupled respiration. The OCR before oligomycin injection was set as 100% (*n* = 3/group). The data are presented as mean ± SEM. *, P < 0.05; **, P < 0.01; ***, P < 0.001 by two-tailed Student's *t* test (A–C [bottom], E, F and G [right], H, I [right], J, and K [right]). Data are representative of at least two (A–D, F, and K) or three independent experiments (E, H, and J). Veh, vehicle; R/A, Rotenone/Antimycin A; FCCP, Trifluoromethoxy carbonylcyanide phenylhydrazone.

uptake ($VO_2$), EE, RER, and locomotor activity were measured in a resting state using the PhenoMaster System (TSE Systems GmbH). For the experiment, the mice first acclimated for 8 h in a metabolic chamber provided with food and water were subsequently evaluated for 3 d. The temperature for these studies was kept at 22°C or 30°C with a 12-h light/dark cycle. Standard in-house software was used to measure the EE.

### Cold tolerance test

A cold tolerance test was performed in 8–9-wk-old mice. The animals were subjected to a cold room (4–8°C) without access to food or water. The rectal temperature was measured at the indicated time after exposure to cold using a Testo 925 electronic rectal thermometer (Testo).

### Measurement of body mass

Fat and lean body masses were measured by 1H magnetic resonance spectroscopy (Bruker BioSpin).

### Measurement of surface body temperature

A thermal camera (FLIR Systems) was used to measure surface body temperature of control and *Pld2* Ad-KO mice. During capture of thermal images, mice behavior was controlled to avoid artificial effects. Surface temperature is calculated as the highest area of the BAT using thermal imaging.

### Measurement of blood glucose and plasma insulin levels

For the oral-glucose tolerance test (O-GTT), 10-h overnight-fasted mice were injected with 2 g of glucose (Sigma-Aldrich) per kg of body weight via oral injection. After the injection, blood was taken by puncturing of the tail vein, and glucose levels were measured using a glucometer (Roche) at the indicated time points. For the insulin tolerance test (ITT), 10-h overnight-fasted mice were injected with human insulin (Santa Cruz Biotechnology; 0.75 U/kg body weight) via i.p. injection, and tail blood glucose concentrations were monitored at the indicated time points. Plasma insulin concentrations were determined in 10-h overnight-fasted mice using ELISA kits (ALPCO).

### CAY10594 injection in mice

CAY10594 (Cayman Chemical) was dissolved in DMSO/Tween-80/distilled water (1:1:8). This working solution was mixed by vortexing and i.p.-injected at a dosage of 10 mg/kg CAY10594. Control groups were injected with equal volumes of DMSO diluted in the distilled water and Tween-80 solution, and weekly body weight was measured. After 10 wk of injection, O-GTT, ITT, and metabolic rate were measured as described above.

### Cell culture

ingWAT and BAT were isolated from 6-wk-old C57BL/6J mice. Briefly, the ingWAT was minced and digested with 1.5 mg/ml collagenase in 10% FBS DMEM, and BAT was reacted with 1.5 mg/ml collagenase in 10 mM $CaCl_2$ PBS for 30 min at 37°C with constant shaking. Mature adipocytes and connective tissues were separated from the cell pellet by centrifugation at 200 *g* for 5 min. The cell pellet was then suspended with ACK lysis buffer (Invitrogen) and filtered through a 100-μm cell strainer (BD Bioscience). After PBS washing, the pelleted stromal vascular cells from ingWAT were resuspended in DMEM/F12 containing 10% FBS and 1% penicillin/streptomycin (P/S) and seeded in 6-well plates for adipogenic differentiation. 90–95% confluent cells were differentiated with a medium containing 5% FBS, 10 μg/ml insulin, 120 μM indomethacin, 0.2 μM dexamethasone, 0.5 mM 3-isobutyl-1-methylxanthine, 1 nM 3,3′,5-triiodo-l-thyronine, and 1% P/S. After 3 d, the medium was replaced with maintenance medium containing 10% FBS, 10 μg/ml insulin, and 1% P/S. After 2 d, these cells were maintained in DMEM/F12 with 10% FBS and 1% P/S. To prepare the brown adipocytes, washed stromal vascular cells from BAT were resuspended in DMEM containing 20% FBS and 1% P/S and seeded in 6-well plates. 90–95% confluent cells were differentiated with a DMEM medium containing 10% FBS, 125 μM indomethacin, 2 μg/ml dexamethasone, 0.5 mM 3-isobutyl-1-methylxanthine, 0.5 μM rosiglitazone, and 1% P/S. After 3 d, the medium was replaced with maintenance medium containing 15% FBS, 10 μg/ml insulin, 1 nM 3,3′,5-triiodo-l-thyronine, and 1% P/S. After 2 d, these cells were maintained in DMEM with

20% FBS and 1% P/S. The medium was refreshed every 2 d until the cells were fully differentiated at day 7. To test the effect of CAY10594 to adipocyte differentiation, the adipocytes were treated with DMSO or 10 µM CAY10594 (Cayman Chemical) in the induction stage for 5 d.

### Mitochondrial respiration analysis

Stromal vascular fraction was isolated from ingWAT or BAT and determined using a Seahorse XF24 Extracellular Flux Analyzer. Cells were seeded and differentiated in XF 24-well cell culture microplates (Agilent) at 1.0 × $10^5$ cells per well in 500 µl of growth medium. In the palmitate-BSA–containing media (Agilent), respiration was assessed at the basal state, and under CAY10594 treatment (10 µM), 2 µM oligomycin, 1 µM carbonyl cyanide-4-phenylhydrazone, and 0.5 µM rotenone/antimycin A were added at 22-min intervals. Consumption values were normalized to extracted protein from the cell lysate of the final mixture. The oxygen consumption test was repeated two times for each replicate.

### Confocal microscopy

For the visualization of PLD2 inhibitor (CAY10594)–induced colocalization of p62 and mitochondria, primary adipocytes were seeded onto coverslips in 6-well plates. The cells were fixed in 3% paraformaldehyde for 15 min and permeabilized in 0.1% Triton X-100 in PBS for 5 min at room temperature. After incubation with PBS containing 2% BSA for 20 min, the samples were incubated with a mouse monoclonal antibody against TOM20 (1:200; Santa Cruz Biotechnology) and rabbit polyclonal antibody against p62 (1:500, Abcam) for 3 h at room temperature. The samples were washed with PBS three times, incubated with secondary antibody for 2 h, and counterstained with DAPI (Invitrogen) for 15 min. The coverslips were mounted onto glass slides and visualized by a Zeiss LSM700 microscope. The images acquired were processed with Adobe Photoshop. Colocalization was performed using ImageJ Software (National Institutes of Health).

### Transmission electron microscopy

The tissues were initially fixed for 2 h with 2.5% glutaraldehyde in 0.1 M phosphate (pH 7.3) at room temperature. After fixation, the tissues were treated with 1% $OsO_4$ plus 1.5% potassium ferrocyanide in 0.1 M phosphate buffer (pH 7.3) for 1 h at 4°C in the dark and embedded in epon 812 after dehydration in an ethanol and propylene oxide series. Polymerization was conducted using pure resin at 70°C for 2 d. Ultrathin sections (70 nm) were obtained with an ultramicrotome (EM UC7; Leica), then collected on 100-mesh copper grids. After staining with 2% uranyl acetate (15 min) and lead citrate (5 min), the sections were examined by transmission electron microcopy at 120 kV (JEM-1400Plus) at the Korea Basic Science Institute. Mitochondrial number, area, and cristae length measurements were performed using ImageJ (National Institutes of Health).

### Flow cytometry analysis for mitochondria

Matured brown adipocytes from BAT of WT mice were incubated with 1% (wt/vol) fatty acid–free low-endotoxin BSA (Sigma-Aldrich)–conjugated palmitate (Sigma-Aldrich) for mitochondrial stress. After incubation, adipocytes were stimulated with DMSO or 10 µM CAY10594 for 3 or 24 h in an incubator at 37°C. Stimulated cells were stained with 100 nM of TMRM (Thermo Fisher Scientific) for 30 min at 37°C. The cells were then washed with PBS twice and analyzed using a FACSCanto II (BD Biosciences) and FlowJo (TreeStar) software.

### Statistical analysis

All results were evaluated using GraphPad prism software. Statistical analysis was performed using Student's *t* test or ANOVA. All results are expressed as mean ± SEM. P values <0.05 are considered statistically significant.

### Online supplemental material

Fig. S1 shows the effects of HFD or isoprenaline on *Pld2* mRNA levels in ingWAT, BAT, and brown adipocytes and on metabolic parameters in adipocyte-specific *Pld2* KO or PLD2-inhibited mice. Fig. S2 shows metabolic parameters and insulin sensitivity of PLD2-inhibited or adipocyte PLD2-ablated mice. Fig. S3 shows changes in p62, UCP1, Drp1, Fis1, LC3B, and mitochondrial condition in PLD2-inhibited or adipocyte *Pld2*-ablated mice. Table S1 shows primer sequences used for quantitative RT-PCR.

### Data availability

All data needed to evaluate the conclusions in the paper are present in the paper and the online supplemental material.

## Acknowledgments

We thank Dr. Su Myung Jung (Sungkyunkwan University) for his helpful discussions and Dr. Hyunsoo Kim (Sungkyunkwan University) for his helpful statistical analysis.

This study was supported by the National Research Foundation of Korea funded by the Ministry of Science ICT and Future Planning through the Basic Science Research Program Planning (NRF-2021R1A2C3011228, NRF-2017R1A5A1014560) and Korea Mouse Phenotyping Project (2013M3A9D5072550).

Author contributions: H. Kim, M. Park, and Y. Bae conceived the study, planned the experiments, and collected all data. H. Kim, M. Park, N. Yun, H. Go, and M. Kim performed experiments and analyzed data. J. Seong, M. Lee, E. Kang, J. Ghim, and S. Ryu planned experiments and supported resources. H. Kim, M. Park, B.A. Zabel, A. Koh, and Y. Bae wrote the first version of the manuscript. All authors have critically revised and approved the final version.

Disclosures: H.S. Kim, Y.-S. Bae, and M.Y. Park reported a patent to 10-2324725 (Korea) issued and a patent to PCT/KR2021/006807 pending. Y.-S. Bae reported grants from National Research Foundation of Korea during the conduct of the study. No other disclosures were reported.

Submitted: 17 July 2021
Revised: 18 November 2021
Accepted: 8 December 2021

## References


Al-Goblan, A.S., M.A. Al-Alfi, and M.Z. Khan. 2014. Mechanism linking diabetes mellitus and obesity. *Diabetes Metab. Syndr. Obes.* 7:587–591. https://doi.org/10.2147/DMSO.S67400

Ali, D.C., M. Naveed, A. Gordon, F. Majeed, M. Saeed, M.I. Ogbuke, M. Atif, H.M. Zubair, and L. Changxing. 2020. β-Adrenergic receptor, an essential target in cardiovascular diseases. *Heart Fail. Rev.* 25:343–354. https://doi.org/10.1007/s10741-019-09825-x

Bartelt, A., S.B. Widenmaier, C. Schlein, K. Johann, R.L.S. Goncalves, K. Eguchi, A.W. Fischer, G. Parlakgül, N.A. Snyder, T.B. Nguyen, et al. 2018. Brown adipose tissue thermogenic adaptation requires Nrf1-mediated proteasomal activity. *Nat. Med.* 24:292–303. https://doi.org/10.1038/nm.4481

Bazzano, L.A., D. Gu, M.R. Whelton, X. Wu, C.S. Chen, X. Duan, J. Chen, J.C. Chen, and J. He. 2010. Body mass index and risk of stroke among Chinese men and women. *Ann. Neurol.* 67:11–20. https://doi.org/10.1002/ana.21950

Becher, T., S. Palanisamy, D.J. Kramer, M. Eljalby, S.J. Marx, A.G. Wibmer, S.D. Butler, C.S. Jiang, R. Vaughan, H. Schöder, et al. 2021. Brown adipose tissue is associated with cardiometabolic health. *Nat. Med.* 27:58–65. https://doi.org/10.1038/s41591-020-1126-7

Blaszkiewicz, M., and K.L. Townsend. 2016. Adipose tissue and energy expenditure: central and peripheral neural activation pathways. *Curr. Obes. Rep.* 5:241–250. https://doi.org/10.1007/s13679-016-0216-9

Bournat, J.C., and C.W. Brown. 2010. Mitochondrial dysfunction in obesity. *Curr. Opin. Endocrinol. Diabetes Obes.* 17:446–452. https://doi.org/10.1097/MED.0b013e32833c3026

Brown, H.A., P.G. Thomas, and C.W. Lindsley. 2017. Targeting phospholipase D in cancer, infection and neurodegenerative disorders. *Nat. Rev. Drug Discov.* 16:351–367. https://doi.org/10.1038/nrd.2016.252

Cannon, B., and J. Nedergaard. 2004. Brown adipose tissue: function and physiological significance. *Physiol. Rev.* 84:277–359. https://doi.org/10.1152/physrev.00015.2003

Cannon, B., and J. Nedergaard. 2011. Nonshivering thermogenesis and its adequate measurement in metabolic studies. *J. Exp. Biol.* 214:242–253. https://doi.org/10.1242/jeb.050989

Chaudhry, A., and J.G. Granneman. 1999. Differential regulation of functional responses by β-adrenergic receptor subtypes in brown adipocytes. *Am. J. Physiol.* 277:R147–R153. https://doi.org/10.1152/ajpregu.1999.277.1.R147

Cho, J.H., and J.-S. Han. 2017. Phospholipase D and its essential role in cancer. *Mol. Cells.* 40:805–813.

Choi, J.W., S.M. Son, I. Mook-Jung, Y.J. Moon, J.Y. Lee, K.-C. Wang, H.-S. Kang, J.H. Phi, S.A. Choi, S. Chong, et al. 2018. Mitochondrial abnormalities related to the dysfunction of circulating endothelial colony-forming cells in moyamoya disease. *J. Neurosurg.* 129:1151–1159. https://doi.org/10.3171/2017.5.JNS17147

Chondronikola, M., E. Volpi, E. Børsheim, C. Porter, P. Annamalai, S. Enerbäck, M.E. Lidell, M.K. Saraf, S.M. Labbe, N.M. Hurren, et al. 2014. Brown adipose tissue improves whole-body glucose homeostasis and insulin sensitivity in humans. *Diabetes.* 63:4089–4099. https://doi.org/10.2337/db14-0746

Cohen, P., and B.M. Spiegelman. 2016. Cell biology of fat storage. *Mol. Biol. Cell.* 27:2523–2527. https://doi.org/10.1091/mbc.e15-10-0749

Cypess, A.M., L.S. Weiner, C. Roberts-Toler, E. Franquet Elía, S.H. Kessler, P.A. Kahn, J. English, K. Chatman, S.A. Trauger, A. Doria, and G.M. Kolodny. 2015. Activation of human brown adipose tissue by a β3-adrenergic receptor agonist. *Cell Metab.* 21:33–38. https://doi.org/10.1016/j.cmet.2014.12.009

Ebong, I.A., D.C. Goff Jr., C.J. Rodriguez, H. Chen, and A.G. Bertoni. 2014. Mechanisms of heart failure in obesity. *Obes. Res. Clin. Pract.* 8:e540–e548. https://doi.org/10.1016/j.orcp.2013.12.005

Feldmann, H.M., V. Golozoubova, B. Cannon, and J. Nedergaard. 2009. UCP1 ablation induces obesity and abolishes diet-induced thermogenesis in mice exempt from thermal stress by living at thermoneutrality. *Cell Metab.* 9:203–209. https://doi.org/10.1016/j.cmet.2008.12.014

Fischer, A.W., C. Schlein, B. Cannon, J. Heeren, and J. Nedergaard. 2019. Intact innervation is essential for diet-induced recruitment of brown adipose tissue. *Am. J. Physiol. Endocrinol. Metab.* 316:E487–E503. https://doi.org/10.1152/ajpendo.00443.2018

Fischer, K., A. Fenzl, D. Liu, K.A. Dyar, M. Kleinert, M. Brielmeier, C. Clemmensen, A. Fedl, B. Finan, A. Gessner, et al. 2020. The scaffold protein p62 regulates adaptive thermogenesis through ATF2 nuclear target activation. *Nat. Commun.* 11:2306. https://doi.org/10.1038/s41467-020-16230-8

Foster, D.A., and L. Xu. 2003. Phospholipase D in cell proliferation and cancer. *Mol. Cancer Res.* 1:789–800.

Franco-Iborra, S., and K. Tanji. 2020. Histochemical and immunohistochemical staining methods to visualize mitochondrial proteins and activity. *Methods Cell Biol.* 155:247–270. https://doi.org/10.1016/bs.mcb.2019.11.024

Gambini, E., I. Martinelli, I. Stadiotti, M.C. Vinci, A. Scopece, L. Eramo, E. Sommariva, J. Resta, S. Benaouadi, E. Cogliati, et al. 2020. Differences in Mitochondrial Membrane Potential Identify Distinct Populations of Human Cardiac Mesenchymal Progenitor Cells. *Int. J. Mol. Sci.* 21:7467. https://doi.org/10.3390/ijms21207467

Ghim, J., J.-S. Moon, C.S. Lee, J. Lee, P. Song, A. Lee, J.-H. Jang, D. Kim, J.H. Yoon, Y.J. Koh, et al. 2014. Endothelial deletion of phospholipase D2 reduces hypoxic response and pathological angiogenesis. *Arterioscler. Thromb. Vasc. Biol.* 34:1697–1703. https://doi.org/10.1161/ATVBAHA.114.303416

Gomez-Cambronero, J. 2014. Phosphatidic acid, phospholipase D and tumorigenesis. *Adv. Biol. Regul.* 54:197–206. https://doi.org/10.1016/j.jbior.2013.08.006

Goto, T., M. Kim, H. Takahashi, N. Takahashi, and T. Kawada. 2016. Food Intake and Thermogenesis in Adipose Tissue. *Korean J. Obes.* 25:109–114. https://doi.org/10.7570/kjo.2016.25.3.109

Hall, J.E., J.M. do Carmo, A.A. da Silva, Z. Wang, and M.E. Hall. 2015. Obesity-induced hypertension: interaction of neurohumoral and renal mechanisms. *Circ. Res.* 116:991–1006. https://doi.org/10.1161/CIRCRESAHA.116.305697

Hammerschmidt, P., D. Ostkotte, H. Nolte, M.J. Gerl, A. Jais, H.L. Brunner, H.-G. Sprenger, M. Awazawa, H.T. Nicholls, S.M. Turpin-Nolan, et al. 2019. CerS6-derived sphingolipids interact with Mff and promote mitochondrial fragmentation in obesity. *Cell.* 177:1536–1552.e23. https://doi.org/10.1016/j.cell.2019.05.008

Held, N.M., and R.H. Houtkooper. 2015. Mitochondrial quality control pathways as determinants of metabolic health. *BioEssays.* 37:867–876. https://doi.org/10.1002/bies.201500013

Henkels, K.M., G.P. Boivin, E.S. Dudley, S.J. Berberich, and J. Gomez-Cambronero. 2013. Phospholipase D (PLD) drives cell invasion, tumor growth and metastasis in a human breast cancer xenograph model. *Oncogene.* 32:5551–5562. https://doi.org/10.1038/onc.2013.207

Huang, J., J.F. Linares, A. Duran, W. Xia, A.R. Saltiel, T.D. Müller, M.T. Diaz-Meco, and J. Moscat. 2021. NBR1 is a critical step in the repression of thermogenesis of p62-deficient adipocytes through PPARγ. *Nat. Commun.* 12:2876. https://doi.org/10.1038/s41467-021-23085-0

Inagaki, T., J. Sakai, and S. Kajimura. 2016. Transcriptional and epigenetic control of brown and beige adipose cell fate and function. *Nat. Rev. Mol. Cell Biol.* 17:480–495. https://doi.org/10.1038/nrm.2016.62

Jang, J.-H., C.S. Lee, D. Hwang, and S.H. Ryu. 2012. Understanding of the roles of phospholipase D and phosphatidic acid through their binding partners. *Prog. Lipid Res.* 51:71–81. https://doi.org/10.1016/j.plipres.2011.12.003

Jiang, S.Z., W. Lu, X.F. Zong, H.Y. Ruan, and Y. Liu. 2016. Obesity and hypertension. *Exp. Ther. Med.* 12:2395–2399. https://doi.org/10.3892/etm.2016.3667

Kajimura, S., B.M. Spiegelman, and P. Seale. 2015. Brown and beige fat: physiological roles beyond heat generation. *Cell Metab.* 22:546–559. https://doi.org/10.1016/j.cmet.2015.09.007

Lee, S.K., S.D. Kim, M. Kook, H.Y. Lee, J. Ghim, Y. Choi, B.A. Zabel, S.H. Ryu, and Y.-S. Bae. 2015. Phospholipase D2 drives mortality in sepsis by inhibiting neutrophil extracellular trap formation and down-regulating CXCR2. *J. Exp. Med.* 212:1381–1390. https://doi.org/10.1084/jem.20141813

Levine, J.A., N.L. Eberhardt, and M.D. Jensen. 1999. Role of nonexercise activity thermogenesis in resistance to fat gain in humans. *Science.* 283:212–214. https://doi.org/10.1126/science.283.5399.212

Lindsley, C.W., and H.A. Brown. 2012. Phospholipase D as a therapeutic target in brain disorders. *Neuropsychopharmacology.* 37:301–302. https://doi.org/10.1038/npp.2011.178

Liu, H., C. Dai, Y. Fan, B. Guo, K. Ren, T. Sun, and W. Wang. 2017. From autophagy to mitophagy: the roles of P62 in neurodegenerative diseases. *J. Bioenerg. Biomembr.* 49:413–422. https://doi.org/10.1007/s10863-017-9727-7

Lowell, B.B., and E.S. Bachman. 2003. β-Adrenergic receptors, diet-induced thermogenesis, and obesity. *J. Biol. Chem.* 278:29385–29388. https://doi.org/10.1074/jbc.R300011200

Lowell, B.B., and J.S. Flier. 1997. Brown adipose tissue, β 3-adrenergic receptors, and obesity. *Annu. Rev. Med.* 48:307–316. https://doi.org/10.1146/annurev.med.48.1.307

Lu, Y., H. Fujioka, D. Joshi, Q. Li, P. Sangwung, P. Hsieh, J. Zhu, J. Torio, D. Sweet, L. Wang, et al. 2018. Mitophagy is required for brown adipose

tissue mitochondrial homeostasis during cold challenge. *Sci. Rep.* 8:8251. https://doi.org/10.1038/s41598-018-26394-5

Madamanchi, A. 2007. β-adrenergic receptor signaling in cardiac function and heart failure. *McGill J. Med.* 10:99–104.

Makki, K., P. Froguel, and I. Wolowczuk. 2013. Adipose tissue in obesity-related inflammation and insulin resistance: cells, cytokines, and chemokines. *ISRN Inflamm.* 2013:139239. https://doi.org/10.1155/2013/139239

Mendez-Gomez, H.R., J. Singh, C. Meyers, W. Chen, O.S. Gorbatyuk, and N. Muzyczka. 2018. The lipase activity of phospholipase D2 is responsible for nigral neurodegeneration in a rat model of Parkinson's disease. *Neuroscience.* 377:174–183. https://doi.org/10.1016/j.neuroscience.2018.02.047

Michel, M.C., O.-E. Brodde, and P.A. Insel. 1990. Peripheral adrenergic receptors in hypertension. *Hypertension.* 16:107–120. https://doi.org/10.1161/01.HYP.16.2.107

Michel, L.Y.M., C. Farah, and J.-L. Balligand. 2020. The Beta3 adrenergic receptor in healthy and pathological cardiovascular tissues. *Cells.* 9:2584. https://doi.org/10.3390/cells9122584

Morrison, S.F., C.J. Madden, and D. Tupone. 2014. Central neural regulation of brown adipose tissue thermogenesis and energy expenditure. *Cell Metab.* 19:741–756. https://doi.org/10.1016/j.cmet.2014.02.007

Muir, L.A., C.K. Neeley, K.A. Meyer, N.A. Baker, A.M. Brosius, A.R. Washabaugh, O.A. Varban, J.F. Finks, B.F. Zamarron, C.G. Flesher, et al. 2016. Adipose tissue fibrosis, hypertrophy, and hyperplasia: Correlations with diabetes in human obesity. *Obesity (Silver Spring).* 24:597–605. https://doi.org/10.1002/oby.21377

Müller, T.D., S.J. Lee, M. Jastroch, D. Kabra, K. Stemmer, M. Aichler, B. Abplanalp, G. Ananthakrishnan, N. Bhardwaj, S. Collins, et al. 2013. p62 links β-adrenergic input to mitochondrial function and thermogenesis. *J. Clin. Invest.* 123:469–478. https://doi.org/10.1172/JCI64209

Ohtomo, T., K. Ino, R. Miyashita, M. Chigira, M. Nakamura, K. Someya, N. Inaba, M. Fujita, M. Takagi, and J. Yamada. 2017. Chronic high-fat feeding impairs adaptive induction of mitochondrial fatty acid combustion-associated proteins in brown adipose tissue of mice. *Biochem. Biophys. Rep.* 10:32–38. https://doi.org/10.1016/j.bbrep.2017.02.002

Oliveira, T.G., R.B. Chan, H. Tian, M. Laredo, G. Shui, A. Staniszewski, H. Zhang, L. Wang, T.-W. Kim, K.E. Duff, et al. 2010. Phospholipase d2 ablation ameliorates Alzheimer's disease-linked synaptic dysfunction and cognitive deficits. *J. Neurosci.* 30:16419–16428. https://doi.org/10.1523/JNEUROSCI.3317-10.2010

Orava, J., P. Nuutila, T. Noponen, R. Parkkola, T. Viljanen, S. Enerbäck, A. Rissanen, K.H. Pietiläinen, and K.A. Virtanen. 2013. Blunted metabolic responses to cold and insulin stimulation in brown adipose tissue of obese humans. *Obesity (Silver Spring).* 21:2279–2287. https://doi.org/10.1002/oby.20456

Paulo, E., D. Wu, Y. Wang, Y. Zhang, Y. Wu, D.L. Swaney, M. Soucheray, D. Jimenez-Morales, A. Chawla, N.J. Krogan, and B. Wang. 2018. Sympathetic inputs regulate adaptive thermogenesis in brown adipose tissue through cAMP-Salt inducible kinase axis. *Sci. Rep.* 8:11001. https://doi.org/10.1038/s41598-018-29333-6

Poirier, P., T.D. Giles, G.A. Bray, Y. Hong, J.S. Stern, F.X. Pi-Sunyer, R.H. EckelAmerican Heart Association. Obesity Committee of the Council on Nutrition, Physical Activity, and Metabolism. 2006. Obesity and cardiovascular disease: pathophysiology, evaluation, and effect of weight loss: an update of the 1997 American Heart Association Scientific Statement on Obesity and Heart Disease from the Obesity Committee of the Council on Nutrition, Physical Activity, and Metabolism. *Circulation.* 113:898–918. https://doi.org/10.1161/CIRCULATIONAHA.106.171016

Quatela, A., R. Callister, A. Patterson, and L. MacDonald-Wicks. 2016. The energy content and composition of meals consumed after an overnight fast and their effects on diet induced thermogenesis: a systematic review, meta-analyses and meta-regressions. *Nutrients.* 8:670. https://doi.org/10.3390/nu8110670

Rothwell, N.J., and M.J. Stock. 1979. A role for brown adipose tissue in diet-induced thermogenesis. *Nature.* 281:31–35. https://doi.org/10.1038/281031a0

Saito, M. 2013. Brown adipose tissue as a therapeutic target for human obesity. *Obes. Res. Clin. Pract.* 7:e432–e438. https://doi.org/10.1016/j.orcp.2013.09.001

Saito, M., M. Matsushita, T. Yoneshiro, and Y. Okamatsu-Ogura. 2020. Brown adipose tissue, diet-induced thermogenesis, and thermogenic food ingredients: from mice to men. *Front. Endocrinol. (Lausanne).* 11:222. https://doi.org/10.3389/fendo.2020.00222

Sarwar, R., N. Pierce, and S. Koppe. 2018. Obesity and nonalcoholic fatty liver disease: current perspectives. *Diabetes Metab. Syndr. Obes.* 11:533–542. https://doi.org/10.2147/DMSO.S146339

Seibenhener, M.L., Y. Du, M.-T. Diaz-Meco, J. Moscat, M.C. Wooten, and M.W. Wooten. 2013. A role for sequestosome 1/p62 in mitochondrial dynamics, import and genome integrity. *Biochim. Biophys. Acta.* 1833:452–459. https://doi.org/10.1016/j.bbamcr.2012.11.004

Sidossis, L., and S. Kajimura. 2015. Brown and beige fat in humans: thermogenic adipocytes that control energy and glucose homeostasis. *J. Clin. Invest.* 125:478–486. https://doi.org/10.1172/JCI78362

Steed, P.M., and A.H. Chow. 2001. Intracellular signaling by phospholipase D as a therapeutic target. *Curr. Pharm. Biotechnol.* 2:241–256. https://doi.org/10.2174/1389201013378644

Strazzullo, P., L. D'Elia, G. Cairella, F. Garbagnati, F.P. Cappuccio, and L. Scalfi. 2010. Excess body weight and incidence of stroke: meta-analysis of prospective studies with 2 million participants. *Stroke.* 41:e418–e426. https://doi.org/10.1161/STROKEAHA.109.576967

van der Lans, A.A., J. Hoeks, B. Brans, G.H. Vijgen, M.G. Visser, M.J. Vosselman, J. Hansen, J.A. Jörgensen, J. Wu, F.M. Mottaghy, et al. 2013. Cold acclimation recruits human brown fat and increases nonshivering thermogenesis. *J. Clin. Invest.* 123:3395–3403. https://doi.org/10.1172/JCI68993

Vázquez-Vela, M.E.F., N. Torres, and A.R. Tovar. 2008. White adipose tissue as endocrine organ and its role in obesity. *Arch. Med. Res.* 39:715–728. https://doi.org/10.1016/j.arcmed.2008.09.005

von Essen, G., E. Lindsund, B. Cannon, and J. Nedergaard. 2017. Adaptive facultative diet-induced thermogenesis in wild-type but not in UCP1-ablated mice. *Am. J. Physiol. Endocrinol. Metab.* 313:E515–E527. https://doi.org/10.1152/ajpendo.00097.2017

Wang, X. 1999. The role of phospholipase D in signaling cascades. *Plant Physiol.* 120:645–652. https://doi.org/10.1104/pp.120.3.645

Ye, J. 2013. Mechanisms of insulin resistance in obesity. *Front. Med.* 7:14–24. https://doi.org/10.1007/s11684-013-0262-6

Zhang, L., C.K. Ip, I.J. Lee, Y. Qi, F. Reed, T. Karl, J.K. Low, R.F. Enriquez, N.J. Lee, P.A. Baldock, and H. Herzog. 2018. Diet-induced adaptive thermogenesis requires neuropeptide FF receptor-2 signalling. *Nat. Commun.* 9:4722. https://doi.org/10.1038/s41467-018-06462-0

# Supplemental material

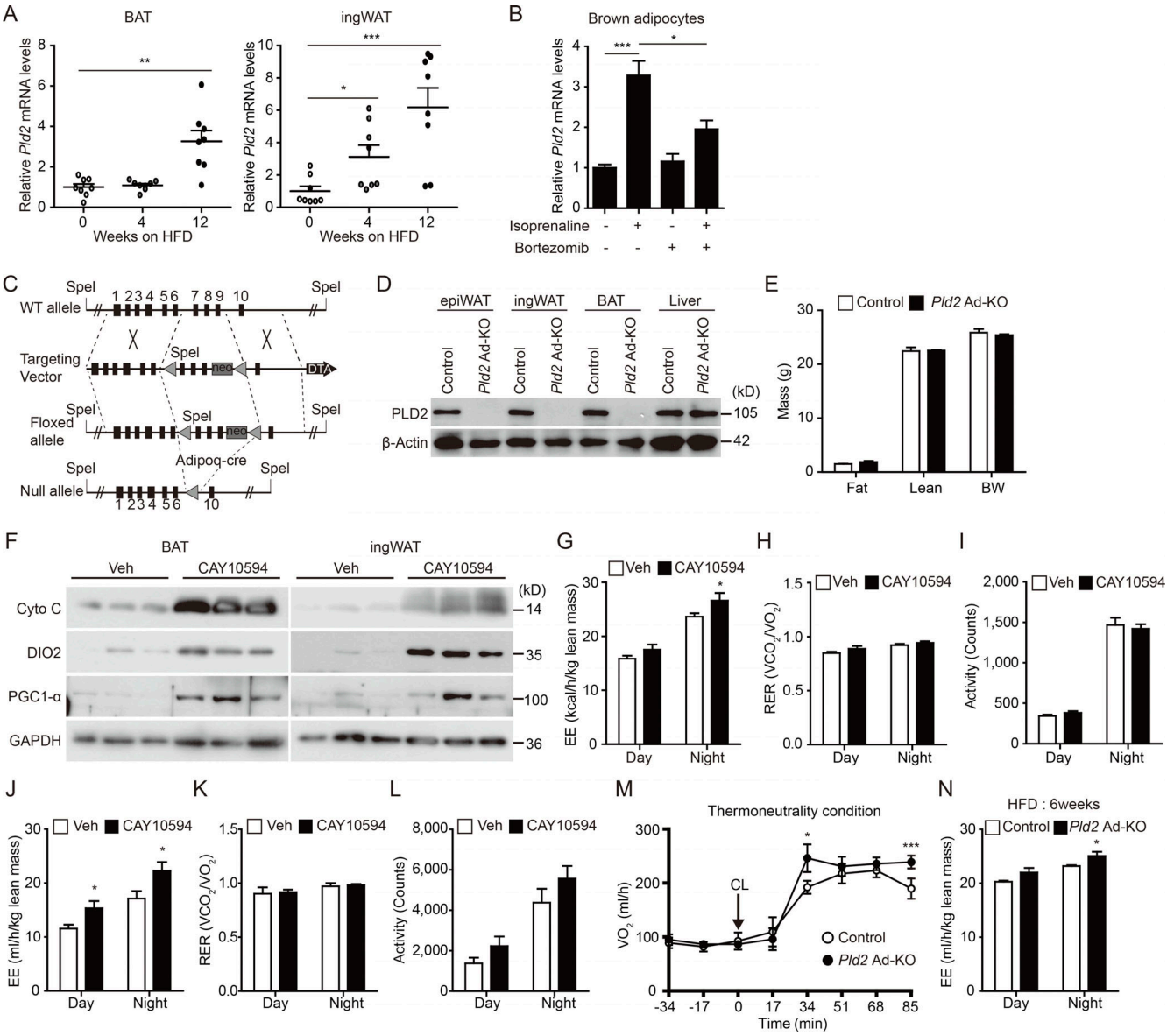


Figure S1. **Effects of HFD or isoprenaline on *Pld2* mRNA levels in ingWAT, BAT, and brown adipocytes and on metabolic parameters in adipocyte-specific *Pld2* KO or PLD2-inhibited mice. (A)** *Pld2* mRNA expression in BAT and ingWAT from HFD-fed mice for 0, 4, and 12 wk ($n$ = 6/group). **(B)** Quantitative RT-PCR for *Pld2* mRNA expression in vehicle- or isoprenaline (1 µM)- or bortezomib (20 nM, 1 h pretreat)-treated primary brown adipocytes for 24 h ($n$ = 4/group). **(C)** Generation of *Pld2* Ad-KO mice. Details of the KO generation strategy are described in the Materials and methods section. **(D)** Western blot analysis of PLD2 and β-Actin in various adipose tissue depots and liver from 8-wk-old control and *Pld2* Ad-KO mice. **(E)** Fat and lean mass, and body weight (BW) of 8-wk-old control and *Pld2* Ad-KO mice ($n$ = 6/group). **(F)** Representative Western blot images of Cytochrome C (Cyto C), DIO2, PGC1-α, and GAPDH in BAT and ingWAT of 8-wk-old mice injected with vehicle or CAY10594 for 7 consecutive days at 22°C. **(G–I)** The level of EE (G), RER (H), and locomotor activity (I) of 8-wk-old mice injected with vehicle or CAY10594 for 7 consecutive days at 22°C ($n$ = 5/group). **(J–L)** The level of EE (J), RER (K), and locomotor activity (L) of 8-wk-old mice injected with vehicle or CAY10594 for 7 consecutive days at 30°C ($n$ = 5/group). **(M)** Oxygen uptake ($VO_2$) levels of CL-injected 8-wk-old control or *Pld2* Ad-KO mice at thermoneutral condition ($n$ = 6/group). **(N)** EE of HFD-fed (6 wk) control and *Pld2* Ad-KO mice ($n$ = 5/group). The data are presented as mean ± SEM. *, P < 0.05; **, P < 0.01; ***, P < 0.001 by two-tailed Student's $t$ test (A, B, E, G–L, and N) and two-way ANOVA (M). Data are representative of two (B and F) or three independent experiments (A and D). Veh, vehicle; $VCO_2$, carbon dioxide production.

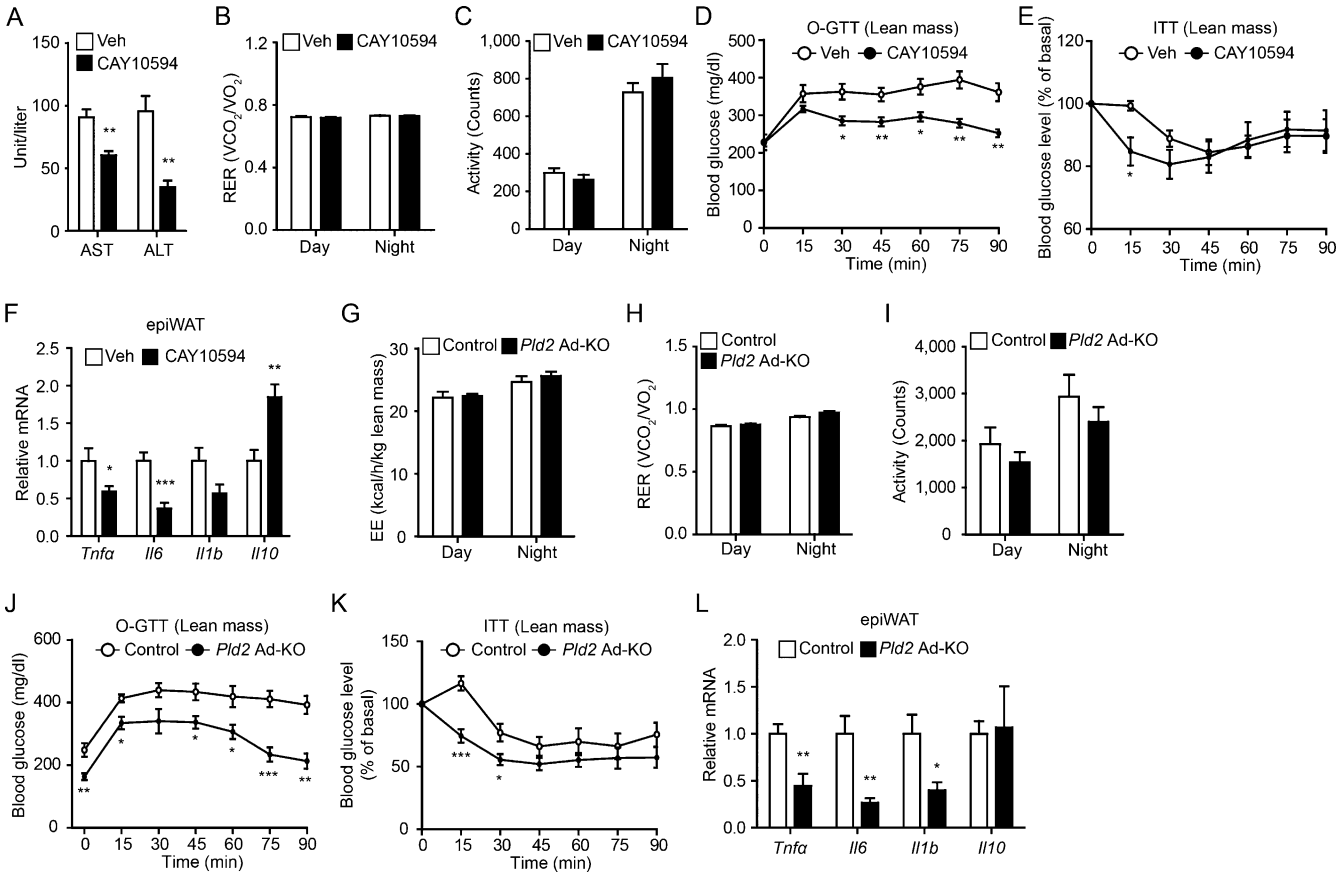


Figure S2. **Metabolic parameters and insulin sensitivity of PLD2-inhibited or adipocyte PLD2-ablated mice. (A–C)** The levels of plasma AST and ALT (A), RER (B), and locomotor activity (C) of vehicle- or CAY10594-injected obese mice (*n* = 6/group). **(D and E)** Blood glucose concentrations during O-GTT (D) and ITT (E) based on lean mass in fasted vehicle- or CAY10594-injected obese mice (*n* = 6/group). **(F)** Inflammation-related gene expression in epiWAT from vehicle and CAY10594-injected obese mice (*n* = 6/group). **(G–I)** The level of EE (G), RER (H), and locomotor activity (I) of HFD-fed (12 wk) control and *Pld2* Ad-KO mice (*n* = 6/group). **(J and K)** Blood glucose concentrations during O-GTT (J) and ITT (K) based on lean mass in HFD-fed (12 wk) control and *Pld2* Ad-KO mice (*n* = 6/group). **(L)** Inflammation-related gene expression in epiWAT from HFD-fed (12 wk) control and *Pld2* Ad-KO mice (*n* = 6/group). The data are presented as mean ± SEM. *, P < 0.05; **, P < 0.01; ***, P < 0.001 by two-tailed Student's *t* test (A–C, F–I, and L) and two-way ANOVA (D, E, J, and K). Data are representative of two (A, F, and L) or three independent experiments (D, E, J, and K). Veh, vehicle.

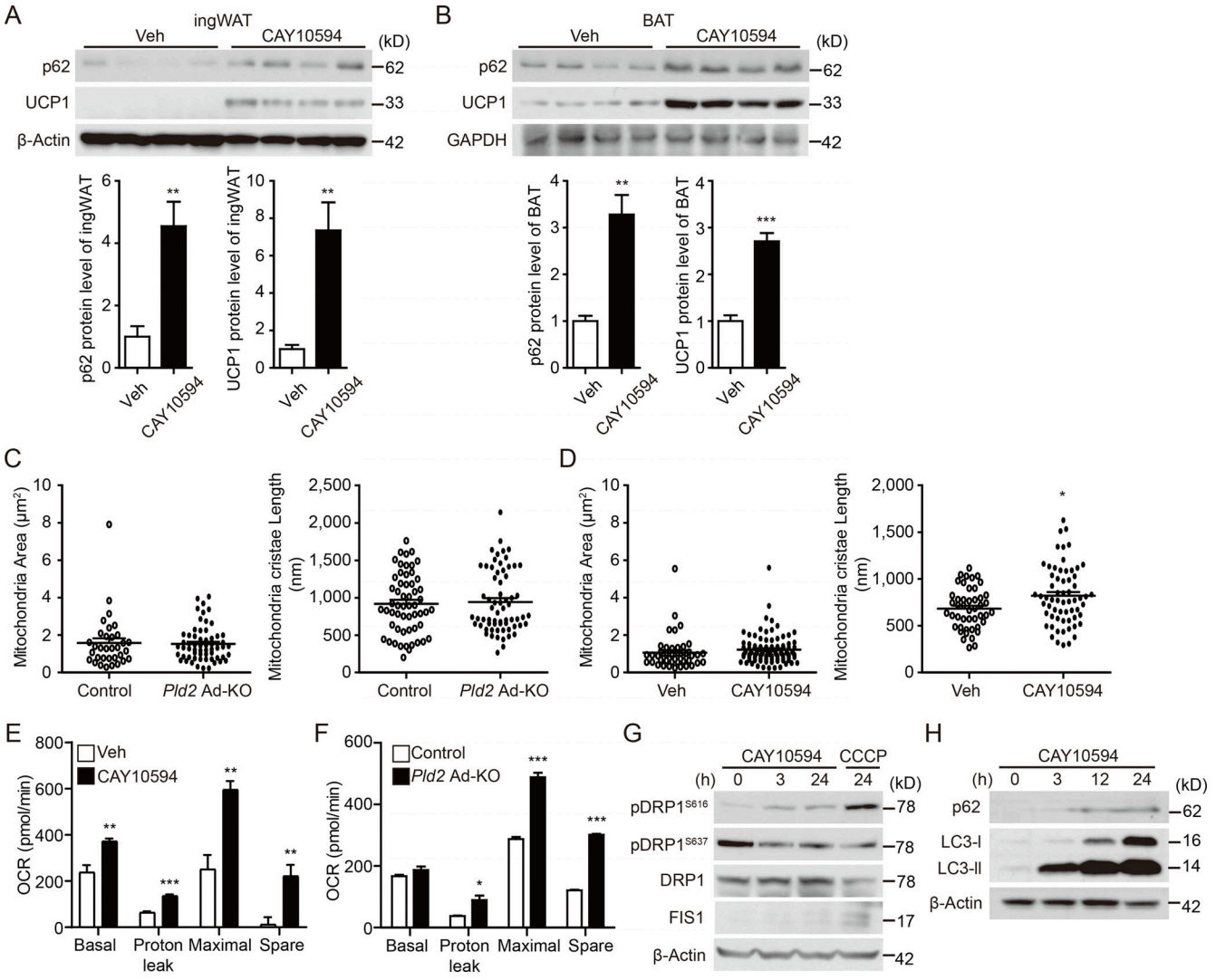


Figure S3. **Changes in p62, UCP1, DRP1, FIS1, LC3B, and mitochondrial condition in PLD2-inhibited or adipocyte *Pld2*-ablated mice. (A and B)** Representative Western blot images (top) and quantification (bottom) of p62, UCP1, and β-Actin, or GAPDH in ingWAT (A) and BAT (B) from vehicle- or CAY10594-injected obese mice ($n$ = 4/group). **(C)** The area (left) and cristae length (right) of mitochondria in BAT from HFD-fed (12 wk) control and *Pld2* Ad-KO mice ($n$ = 6/group). **(D)** The area (left) and cristae length (right) of mitochondria in BAT from vehicle- or CAY10594-injected obese mice ($n$ = 6/group). **(E)** Representative seahorse extracellular flux assays measuring OCR in primary brown adipocytes treated with vehicle or CAY10594 (10 μM) for 5 d ($n$ = 3/group). **(F)** Representative seahorse extracellular flux assays measuring OCR in primary brown adipocytes from control and *Pld2* Ad-KO mice ($n$ = 3/group). **(G)** Representative Western blot images of pDRP1$^{S616}$, pDRP1$^{S637}$, DRP1, FIS1, and β-Actin in primary brown adipocytes treated with CAY10594 (10 μM) and carbonyl cyanide m-chlorophenylhydrazone (CCCP; 20 μM) for the indicated time lengths. **(H)** Representative Western blot images of p62, LC3B, and β-Actin in primary brown adipocytes treated with CAY10594 (10 μM) for the indicated time lengths. The data are presented as mean ± SEM. *, P < 0.05; **, P < 0.01; ***, P < 0.001 by two-tailed Student's $t$ test (A [bottom], B [bottom], and C–F). Data are representative of two (G and H) or three independent experiments (A and B). Veh, vehicle.

**Table S1 is provided as a separate file online. Table S1 shows primer sequences used for quantitative RT-PCR.**